Fire Technology, 49, 293–327, 2013

DOI: 10.1007/s10694-012-0265-x

Advanced Modeling of Composite Slabs with Thin-Walled Steel Sheeting Submitted to Fire

Daphne Pantousa and Euripidis Mistakidis, Laboratory of Structural Analysis and Design, Department of Civil Engineering, University of Thessaly, Pedion Areos, 38334 Volos, Greece*

Received: 24 October 2011/**Accepted:** 10 April 2012

Abstract. The paper studies the behavior of composite slabs with corrugated steel sheeting at elevated temperatures. Two structural systems are considered: a simply supported composite slab and a continuous composite slab that consists of two equal spans. Both of them are designed according to the respective Eurocodes to have similar strengths at room temperature. In the sequel, sophisticated three-dimensional models of the slabs are developed. Coupled thermo-mechanical analysis is used, which takes into account the various nonlinearities that are present in the physical model (dependence of the thermal and mechanical properties of the material on temperature, nonlinear material behavior, cracking etc.). The results of the thermal analysis are compared with the temperature field that is proposed in Eurocode 4. For both the structural systems, the fire resistance, in time domain, that yields from the coupled analysis is compared with the fire resistance that results following the provisions of Eurocode 4. Another objective is to evaluate the effect of static indeterminacy on the fire resistance of composite slabs.

Keywords: Fire resistance, Composite slabs, Numerical modeling

1. Introduction

Composite slabs made with corrugated steel sheeting are commonly used nowadays for the covering of large spans. With respect to ordinary reinforced concrete slabs, they exhibit a number of advantages, as e.g. the ability for the casting of concrete without additional scaffold structures, ease of construction etc. However, concerning fire resistance, they exhibit a significant drawback with respect to reinforced concrete slabs, due to the fact that the corrugated steel sheeting may be directly exposed to fire and, consequently, lose quickly its mechanical properties (stiffness and strength degradation). For this reason, additional reinforcement is usually used in order to ensure that the slab will retain its robustness for the amount of time required by the various fire design codes.

The last decades the research on the fire behavior of composite slabs is focused mainly on experimental studies. A lot of fire tests have been conducted in order to

* Correspondence should be addressed to: Euripidis Mistakidis, E-mail: emistaki@uth.gr

study the fire behavior of composite slabs as individual structural members [1–4]. The most important full scale fire tests, in terms of understanding the structural behavior of composite slabs, were carried out in the Cardington laboratory in the UK. The later tests indicated that the steel–concrete slabs have an important contribution to the prevention of the collapse of the structure. Since the fire tests are very expensive, the research nowadays is usually carried out through numerical methods. Various research studies referred to the Cardington fire tests, used numerical simulations in order to determine the fire performance of the slabs (see e.g. [5, 6]).

For the numerical simulation of the behavior of composite slabs, various models have been proposed in the literature. A numerical model was proposed in [6] in order to predict the fire performance of orthotropic composite slabs. For this purpose a layered slab element was used in order to simulate the concrete. The steel reinforcement was modeled through a smeared steel layer. The numerical analysis was conducted with the well-known software package Vulcan [7].

A model for the simulation of an orthotropic slab in fire was proposed in [8], which was again developed within the software code Vulcan. In order to obtain the real temperature distribution within the slab, the upper continuous portion of the profile was modeled through layered isoparametric slab elements. In this respect the temperature of each layer of the slab was not necessarily uniform in the horizontal plane and it was assumed that temperature can vary between different Gauss integration points. A frame element was used to represent a group of ribs of the slab. The width of this element was an "equivalent" width, calculated from the geometric properties.

A finite element analysis of the first Cardington test was carried out in [9]. In particular, three-dimensional shell elements were used to model the behavior of the composite slab, which took into account material and geometric non-linearity, as well as curvature and non-linear thermal gradients. This work underlines the effects of thermal expansion during the fire exposure. A more accurate thermal analysis of composite slabs was performed in [10], where a finite element adaptive heat transfer program was used. This model took into account the temperature differential between the hot steel metal deck and cold concrete, as well as the air gaps that arise between the materials. This problem was modeled using interface elements between the concrete and the steel profile.

Finally, the failure assessment of lightly reinforced floor slabs under elevated temperature is investigated in [11]. Both a finite element model and a simplified one are developed in this study. The finite element model uses a special 2D shell element implemented in ADAPTIC, while the simplified analytical model takes into account the influence of bond between the steel reinforcement and concrete. The validity of the models is examined through the appropriate validation against experimental results.

In the present paper a numerical model is developed to assist the evaluation of the behavior of composite slabs in elevated temperatures, which is based on the coupling of three-dimensional solid elements that model the concrete with 4-node shell elements that model the steel profile. Reinforcing steel bars are modeled through three-dimensional frame elements. The model is able to take accurately

into account the effects of the increased temperature. The temperatures in the corrugated steel sheeting and in the mass of the slab are calculated by considering accurately the parameters that affect the thermal problem. The thermal loading is applied on the lower side of the slab and follows the standard ISO 834 fire curve adopted by Eurocode 1 [12]. The thermal and structural material properties in elevated temperature are taken into account according to the respective Eurocodes.

The basic objective of this study is to assess the thermal behavior of composite slabs through both simple and advanced calculation models and compare their results. More specifically, the results of the thermo-mechanical analysis, in terms of fire resistance, are compared with the expected fire resistance that results following the provisions of Eurocode 4, Part 1–2 [13]. Despite the significantly simplified procedure proposed by this norm, its application in the case of continuous composite slabs requires the involvement of a nonlinear iterative procedure. The comparison is performed mainly in order to evaluate the effectiveness of simplified methods that are based on the proposals of Eurocode 4. Moreover, the results of the thermal analysis which is conducted according to the principles of the heat transfer theory, applied through the finite element method, are compared with the temperature profiles for composite slabs proposed by Eurocode 4 [13].

Another objective of the paper is to study the fire performance of the steel–concrete slabs considering two structural systems: a simply supported and a two span continuous one. The two systems are designed to have the same load bearing capacity at room temperature. Therefore, the goal here is to evaluate the effect of static indeterminacy on the fire resistance of composite slabs.

The paper is organized as follows. Section 2 presents the fundamentals of the heat transfer theory, on which the coupled numerical analysis is based. Section 3 presents the considered problem and its design for room temperature. Section 4 presents procedures for determining the fire resistance using simplified methods and following the provisions of Eurocode. Section 5 presents in detail the advanced numerical method, while the Sect. 6 presents the obtained results, which are compared against those obtained through the simplified methods of Sect. 5. Finally, in the ''Appendix'' section, the proposed numerical procedure is applied for the simulation of an experimental test included in [14]. The comparison between numerical and experimental results shows a good agreement, validating therefore the proposed numerical methodology.

2. Elements of Heat Transfer Theory

The fundamentals of the heat transfer problem that is treated in this study are first briefly presented. The description is limited only to slabs made with corrugated steel sheeting and concrete and, in particular, to the case that the slab is exposed to fire beneath it.

2.1. Mechanisms of Heat Transfer

The three basic mechanisms of heat transfer that appear in the specific problem examined here are the following:

2.1.1. Convection. Convection is the heat transfer at the interface between a fluid and a solid element. In the case considered here a specific case appears, termed as free or natural convection, in which the heat is transferred by the circulation of fluids (in this case the hot air) due to buoyancy from the density changes induced by the heating itself. Heat transfer through convection takes place only when the fluid (hot air) comes in contact with the steel sheeting of the composite slab.

2.1.2. Radiation. Thermal radiation is the exchange of energy through electromagnetic waves that are emitted from a surface or an object (from the fire to the composite slab in this specific case study). The thermal radiation takes place when the temperature of the materials feeding the fire increases, regardless if they come in contact with the slab. As in the case of light, these electromagnetic waves can be absorbed, transmitted or reflected on the corrugated steel sheeting. Therefore, radiation depends on the orientation of the steel sheeting, its specific shape and on its ability to absorb, transmit and reflect the thermal energy.

2.1.3. Heat Conduction. Since the temperature on the slab volume increases or decreases over time, transient state heat transfer takes place in this case study. The transient state heat conduction partial differential equation is written in the form:

$$k_x \frac{\partial^2 T}{\partial x^2} + k_y \frac{\partial^2 T}{\partial y^2} + k_z \frac{\partial^2 T}{\partial z^2} = \rho C \frac{\partial T}{\partial t}, \tag{1}$$

where k_x, k_y, k_z are the thermal conductivity coefficients of the material in each one of the three spatial directions, ρ is the density of the material and C is its specific heat. All the aforementioned quantities depend on the temperature of the material. Moreover, in the case of porous materials, as e.g. the concrete, the specific heat is affected by the evaporation phenomena that occur over a range of temperatures.

2.2. Boundary Conditions

Boundary conditions should be applied in order to find a solution to Equation 1. According to the nature of the specific problem treated here, these boundary conditions are:

- Adiabatic Boundary Conditions

Adiabatic boundaries can be treated as a special case of the general fixed flux boundary conditions. No heat exchange takes place across such a boundary and the adiabatic boundary condition is written in the form:

$$-k_n \frac{\partial T}{\partial n} = 0. \tag{2}$$

Adiabatic boundaries are used in order to simulate symmetry conditions (no heat exchange takes place along the symmetry axis or surface) or boundaries which are almost completely insulated.

- Boundary Conditions at Solid–Fluid Boundaries

In the case that solid boundaries (steel sheeting or concrete surfaces) are in contact with moving fluids (hot or ambient temperature air), the following boundary condition can be written:

$$-k_n \frac{\partial T}{\partial n} = h(T_s - T_\infty) = h\Delta T, \tag{3}$$

where h is the total heat transfer coefficient and ΔT is the temperature difference between the fluid and the solid boundary surface. In this case T_∞ is the air temperature (assumed as known) and T_s is the temperature of the solid surface, which is not a priori known, but is calculated as a result of the solution process. For cases which are of interest in structural analysis problems, both convective and radiation heat exchange takes place and (3) can be written in the form

$$-k_n \frac{\partial T}{\partial n} = h_c(T_s - T_\infty) + \Phi\varepsilon_r\sigma\left(T_s^4 - T_\infty^4\right), \tag{4}$$

where Φ is the configuration or view factor, ε_r is the resultant emissivity (which depends on the fluid and solid emissivities), σ is the Stefan–Boltzmann constant and h_c is the convective heat transfer coefficient. The first part of the r.h.s. of Equation 4 is known as the convective term whereas the second one is known as the radiative term. The term ε_r can be evaluated by the simple formula

$$\varepsilon_r = \varepsilon_f \times \varepsilon_s, \tag{5}$$

where ε_f is the emissivity of fire (usually taken equal to 1.0) and ε_s is the emissivity of the structural material.

The calculation of the convective heat transfer coefficient h_c depends on the type of the convection that takes place (forced convection or natural convection) and is related to the fluid properties, the orientation of the surface and the type of flow (laminar or turbulent). For the case of the fire-solid boundary conditions, where the natural convection takes place, the flow is turbulent and the h_c can be calculated according to the following equation [15]:

$$h_c = 0,14\left[\left(\frac{g \times \mathrm{P_r}}{T \times v^2}\right)\right]^m k(\Delta T)^m = \alpha(\Delta T)^m, \tag{6}$$

Here ΔT is the temperature difference between the fluid and the solid surface, P_r is the Prandtl number, T is the absolute temperature of the air, v is the relative viscosity of the fluid, k is the thermal conductivity of the air and m is a coefficient

that depends on the side of the structural elements (fire side or ambient temperature air side). Using the appropriate values for P_r, T, v, k for different temperatures and $g = 9.81$ m/sec^2, the value of α can be easily calculated.

For further simplification, Eurocode 1 [12] suggests a constant value for the convective heat transfer coefficient h_c, which depends only on the side of the structural elements (fire side or ambient temperature air side).

3. Description of the Problem: Design at Room Temperature

As explained in Sect. 1, the aim of this study is to evaluate the fire performance of composite slabs through both simple and advanced methods. Two structural systems are considered (see Figure 1): a simply supported composite slab having a span equal to 3.5 m and a continuous composite slab 7 m long, which consists of two equal spans. The dead load of the slabs is $G = 3.97$ kN/m^2, while the live load is taken equal to $Q = 5$ kN/m^2. In both cases the composite slabs are constructed by a trapezoidal steel profile and concrete and they have the same cross-section properties. However, different reinforcement is used, so that the two systems have the same strength at room temperature. The slab has an overall depth of 150 mm. The steel decking is a thin-walled, cold formed profile, made of structural steel FeE320G. It has a depth of 73 mm and a thickness of 1 mm. A normal-weight concrete with calcareous aggregates is used to form the composite slab, which has a compressive strength of 25 MPa and a tensile strength of 2.9 MPa at room temperature. The steel reinforcement has a yield stress equal to 500 MPa.

The design of the slabs at room temperature for the ultimate limit state combination ($1.35G + 1.5Q$) is performed, considering the fact that the load bearing capacity should be the same for both structural systems. The lower reinforcement of the simply supported slab is first determined, assuming a single Ø8 bar at every rib of the composite slab (i.e. Ø8/187.5 mm). This reinforcement is assumed to extend along the total length of the slab for both structural systems. Then, the upper reinforcement of the continuous slab is calculated, so that it leads to hogging moment resistance, M^-_{Rd}, equal to the sagging one, M^+_{Rd}. The calculations give an upper reinforcement demand of Ø12/120 mm. This demand is covered by two groups of reinforcement bars. In the first group, the bars are placed every 240 mm (Ø12/240) and extend along the total length of the continuous slab. In the second group, the bars are placed every 240 mm (Ø12/240) and extend from the mid-length of the left span to the mid-length of the right one. This configuration sums to Ø12/120 over the area of the central support, while the regions near the left and right outer supports remain with Ø12/240. All the reinforcement bars are assumed to have a concrete cover of 30 mm. Table 1 summarizes the structural design at room temperature, for both cases. The design values of the material properties are calculated using the partial safety factors for fire conditions ($\gamma_{M,fi} = 1.0$).

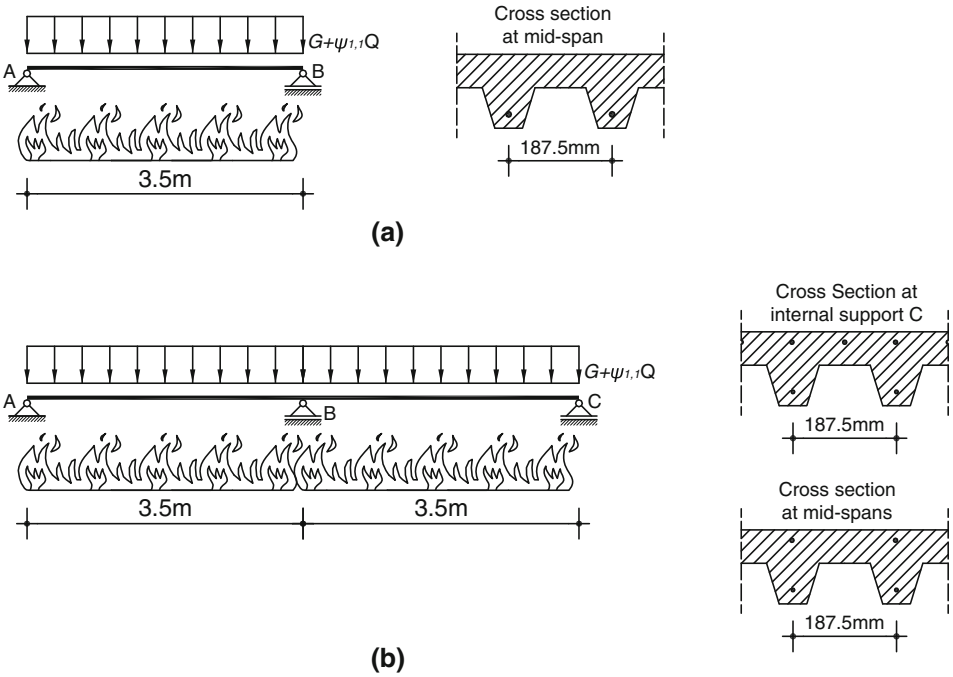

Figure 1. The two systems under study in this paper and the corresponding cross-sections: (a) simply supported slab, (b) the two-span continuous composite slab.

Table 1
Load Bearing Capacities and Amounts of Reinforcement

	M^{+}_{Rd} (kN m/m)	M^{-}_{Rd} (kN m/m)	Lower reinf.	Upper reinf.	Strength utilization (Factor λ)
Simply supported slab	62.72	–	Ø8/187.5	–	0.314
Continuous slab	62.93	57.65	Ø8/187.5	Ø12/120	0.341

With the application of the above design procedure, the two types of slabs have almost the same load bearing capacity at room temperature (the small difference comes from the rounding of the distance between the reinforcements to engineering realistic values). The strength utilization factor λ, which demonstrates the ratio between the design moment to the resistance moment, is almost the same for the two considered slab types and is presented in Table 1.

The fire design is based on the loading combination for accidental design situations given in Eurocode 1 [12] and it can be simplified to $q = G + \psi_{1,1}Q$ (Figure 1). The combination factor $\psi_{1,1}$ is considered here equal to 0.5 according to the Eurocode 0 [16]. This value corresponds to the building categories A and B, i.e. domestic areas or offices.

4. Calculation of the Fire Resistance Through Simplified Models

In this section the fire resistances in the time and strength domains are calculated for both the examined structural systems, using simplified methods. According to Eurocode 4, Part 1–2 [13], the composite slab satisfies the criterion Rx when the load-bearing capacity is maintained for the required x time of fire exposure (x is expressed in minutes). In this study, the critical time t is calculated, in which the design bending moments for the fire situation reach the corresponding resistances of the structural members. This indicates that the load-bearing capacity is maintained for t minutes (the fire resistance is Rt). During this time period the large deformations are acceptable [17]. For the fire, the ISO 834 standard is adopted [13] that prescribes the evolution of the fire temperature over time.

The mechanical properties of concrete and steel that are used in the calculations are taken according to Eurocode 2, Part 1–2 [18] and Eurocode 3, Part 1–2, [19] respectively. It has to be noticed that both the simplified and the advanced calculation models take into account the fact that the yield strength of steel, the compressive strength of concrete and the modulus of elasticity of both materials are temperature dependent.

The determination of the moment resistances in the case of the simplified models is based on the temperature distribution adopted by Eurocode 4 [13]. The calculations here follow the guidelines of [13, Annex D, (Eq. D.2.1)] and result to the diagrams of Figure 2 that depict the calculated temperatures for the upper and lower surfaces of the slab, as a function of the fire time. For convenience, the assumed fire temperatures (ISO curve) are also included in this diagram. Here, it should be noticed that Eurocode 4 [13] gives a procedure for the calculation of the temperatures that is valid only till the 120th minute of fire. However, in order to be able to continue the calculation of the moment resistance beyond this specific point, the results of the heat transfer analysis (Sect. 6.1) are used. This fact explains the "jump" that occurs in the 120th minute in the curve that corresponds to the temperatures of the lower flange of the steel sheeting in Figure 2. The results of the heat transfer analysis are used also for the calculation of the temperatures of the lower reinforcement the web and the upper flange of the steel sheeting.

The determination of the sagging moment resistance $M^{+}_{fi,Rd}$ follows equations (4.2) and (4.3) of [13] that are based on the plastic theory (Figure 3a). At the t-th minute of fire exposure, the temperatures of the various components of the cross-section are assumed to have piecewise uniform values. In this figure, F^{-}_{C} is the compressive force of the concrete, $F^{+}_{S,reinf}$ is the tensile force of the lower reinforcement and $F^{+}_{s,u.f.}$, $F^{+}_{s,web}$, $F^{+}_{s,l.f.}$ are the tensile forces of the upper flange, the web and the lower flange of the steel sheeting respectively. Then, the position of the plastic neutral axis is calculated, on the basis of the equilibrium of the internal forces. Finally, the moment resistance is calculated by the multiplication of each force with the respective lever arm.

The determination of the hogging resistance moment $M^{-}_{fi,Rd}$follows similar principals (Figure 3b). The compressive forces $F^{-}_{s,u.f.}, F^{-}_{s,web}, F^{-}_{s,l.f.}$ of the upper flange,

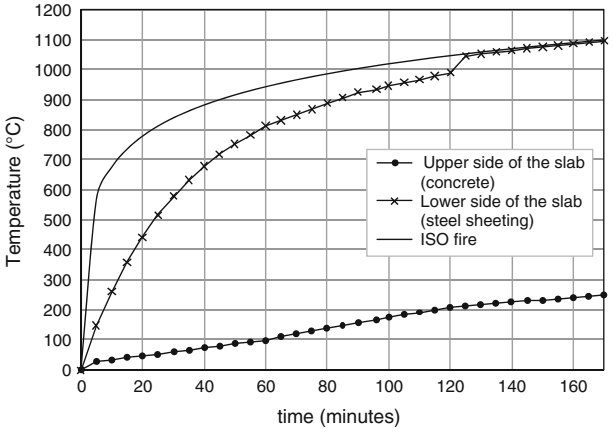

Figure 2. Temperatures at the upper and the lower sides of the composite slab and the ISO fire curve.

the web and lower flange of the steel sheeting can be easily calculated, given the temperatures of the corresponding parts. The tensile force of the upper reinforcement, $F^{+}_{S,reinf}$, is calculated based on the assumption that it is at room temperature. The calculation of the compressive force of concrete is more complex and is based on the method proposed in [13, Annex D, D.3 (7)]. Briefly, an equivalent cross section is defined with a depth equal to h_{eff}, which is divided into n horizontal zones. For each of them the temperature can be calculated, and therefore it is possible to calculate the corresponding forces $F^{-}_{C,Ti}$, $i = 1, \ldots, n$. Finally, the plastic neutral axis and the corresponding moment resistance $M^{-}_{fi,Rd}$ can be easily calculated.

The moment resistances are calculated for the basic module of the slab, which is repeated every 187.5 mm (see Figure 1). However for convenience, an equivalent width of 1 m is considered, therefore in the diagrams of Figure 3 and in the subsequent ones, the moments are given in kNm/m.

4.1. Simply Supported Slab

Taking into account the data given above, it is easily verified that at the 77th minute the design moment resistance $M_{fi,Rd}$ becomes equal to the design moment $M_{fi,Sd}$. Therefore the fire resistance time for the simply supported system is 77 min ($R77$). Figure 4 presents the decrease of the moment resistance $M_{fi,Rd}$ of the simply supported slab with time. The dashed line in the figure represents the design moment $M_{fi,Sd}$.

4.2. Continuous Slab

The case of the continuous slab is more complex, due to the fact that the system is statically indeterminate. In this case, the temperature gradient across the depth of the composite slab creates curvature that cannot be developed freely, producing

(a) Sagging moments

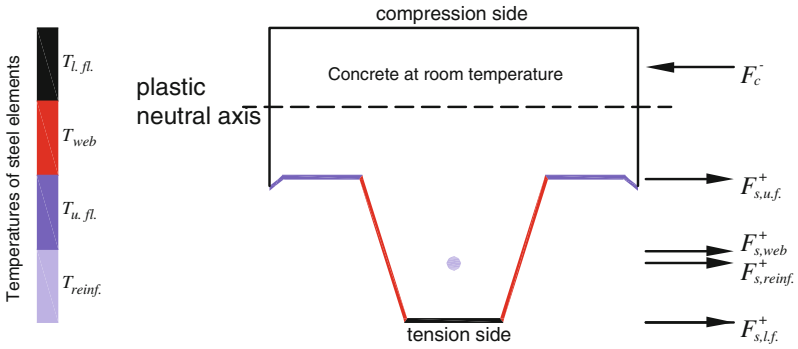

Notes:

1. Concrete under tension is ignored due to the low tensile strength of concrete
2. The upper reinforcement is ignored due to the low contribution to the resistance moment

(b) Hogging moments

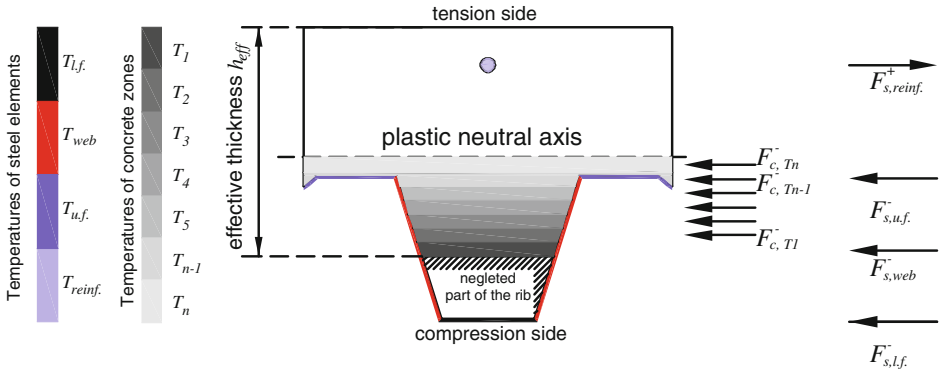

Notes:

1. Concrete under tension is ignored due to the low tensile strength of concrete
2. The lower reinforcement is ignored due to the low contribution to the resistance moment
3. Concrete with temperature greater than T_1 is ignored

Figure 3. Calculation of the sagging and hogging moment resistances according to Eurocode 4.

bending moments. Therefore, in order to calculate the total bending moments that develop along the x-axis of the slab, we have to sum up the bending moments due to the external loading, M_q, and the bending moments due to thermal loading, M_T, i.e.:

$$M_{fi,tot}(x) = M_q(x) + M_T(x) \tag{7}$$

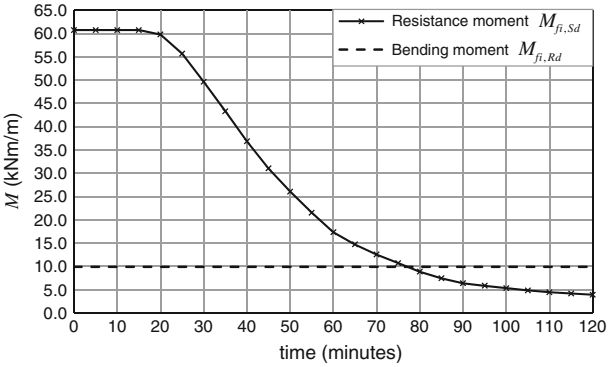

Figure 4. Evolution of the resistance moment at the mid-span of the simply supported slab with time.

Of course, the above equation holds as long as the developed moments are smaller than the corresponding resistances. In order to calculate M_T, it is assumed that the temperature variation across the depth of the slab is linear. The temperature difference is calculated from the curves of Figure 2. Due to the fact that the slab is statically indeterminate, the magnitude of the moments M_T depends on the bending rigidity EJ (where E denotes the modulus of elasticity and J the second moment of inertia of the cross section of the slab). On the other hand, J depends on the value of the developed total bending moment $M_{fi,tot}$, due to the nonlinear behavior of the concrete in tension. Moreover, as the properties of the materials change with temperature, the bending rigidity changes as well. For the above reasons, the calculation of the moment diagram $M_{fi,tot}(x)$ can be obtained only through an iterative process. First, (EJ–M) diagrams were created for characteristic instants of the fire loading (see Figure 5a and 5b) and the length of the continuous slab was discretized into 20 equal frame finite elements. The basic steps of the iterative calculation procedure are given in the sequel. For convenience, the various quantities are equipped with a upper left index denoting the temperature for which the respective quantity occurs, i.e. ${}^{T}M$ denotes the bending moment for the temperature T. The procedure is also demonstrated graphically in Figure 6.

Step 1: Initializations

- Set temperature to room conditions ($T = 20$ °C).
- Select temperature step ΔT (e.g.$\Delta T = 5$ °C).
- Select the accuracy of the iterative procedure ε (i.e. ε is a small number).

Step 2: Calculate the moment distribution $M_q(x)$ due to the fire design load $q = G + \psi_{1,1}Q$.

Step 3: Increase temperature by ΔT and calculate the new temperature T and the temperatures of the upper and lower slab surface (Figure 3).

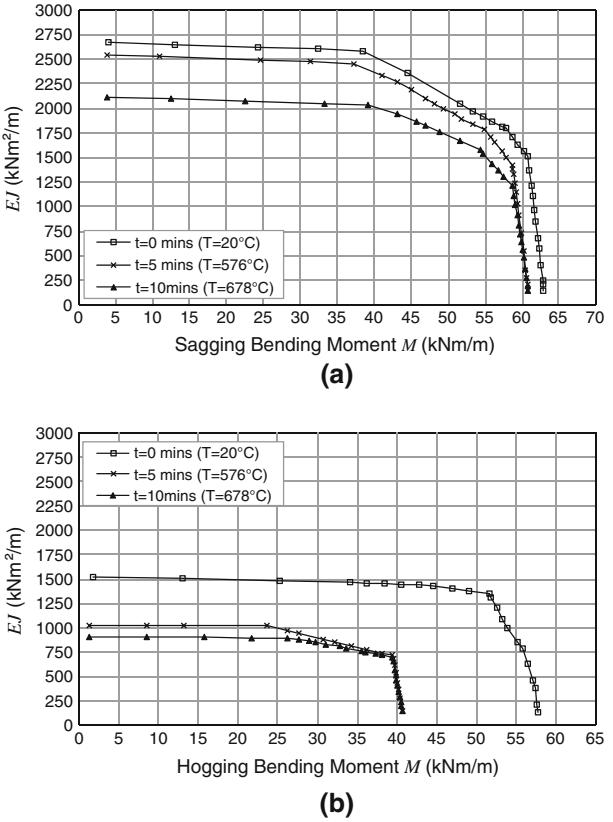

Figure 5. Bending rigidity –moment curves of the slab's cross section at characteristic instants of the fire exposure.

Step 4:

Step 4a

- Set $i = 1$.
- Set as an initial approximation for the moments of the current temperature T, the ones from the previous temperature step, i.e. ${}^{T}M_{fi,tot}^{(1)}(x) = {}^{T-\Delta T}M_{fi,tot}(x)$.

Step 4b

- Calculate the updated rigidities ${}^{T}EJ^{(i)}$ using the appropriate (EJ–M) curve for the temperature T.
- Calculate the moment diagram ${}^{T}M_{T}^{(i)}(x)$ according to the reduced rigidities ${}^{T}EJ^{(i)}$ of the finite element of the slab.
- Calculate the total moment diagram ${}^{T}M_{fi,tot}^{(i)}(x)$ through Equation 7.

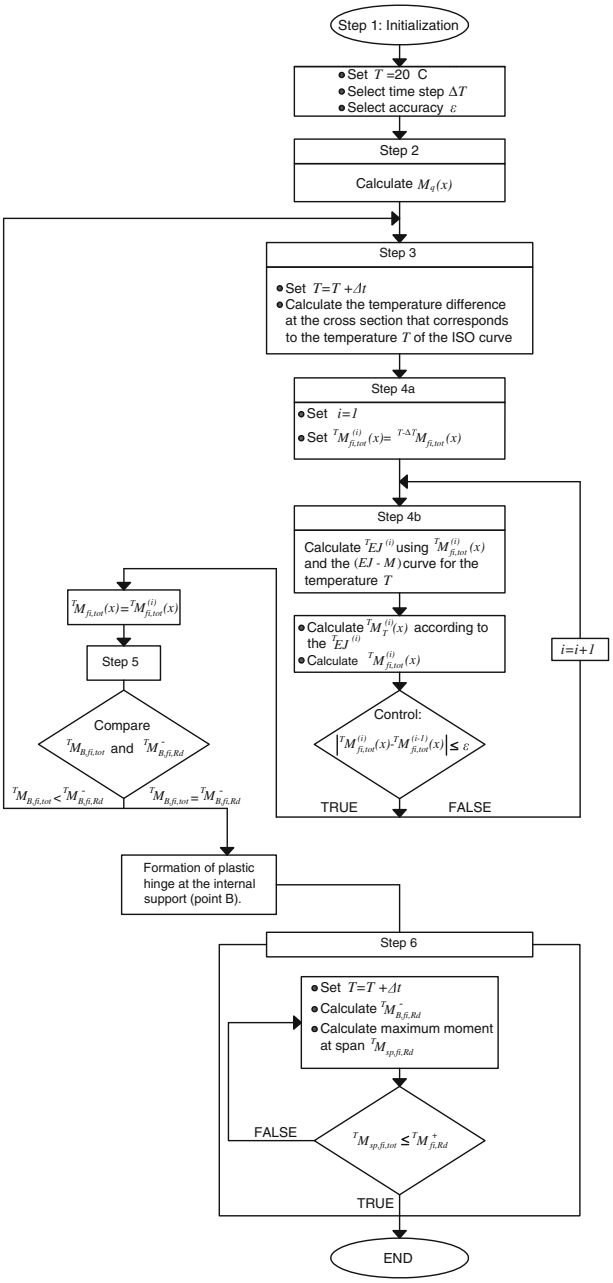

Figure 6. Flowchart for the calculation of the fire resistance according to the simplified method.

- If $\left|{}^{T}M_{fi,tot}^{(i)} - {}^{T}M_{fi,tot}^{(i-1)}\right| \leq \varepsilon$, then the new moment values differ very little from the previous ones, therefore convergence has been attained for temperature T, i.e. ${}^{T}M_{fi,tot}(x) = {}^{T}M_{fi,tot}^{(i)}(x)$. In this case go to Step 5. Else, set $i = i + 1$ and repeat Step 4b.

Step 5: Compare the moment developed at the support B, ${}^{T}M_{B,fi,tot}$, with the corresponding resistance ${}^{T}M_{B,fi,Rd}^{-}$. If ${}^{T}M_{B,fi,tot} < {}^{T}M_{B,fi,Rd}^{-}$, then continue with Step 3. If ${}^{T}M_{B,fi,tot} = {}^{T}M_{B,fi,Rd}^{-}$, then the strength at the support has been exhausted and a plastic hinge is formed at this point. Therefore, from this point on, the slab can be considered as statically determinate and the calculations are simplified because the temperature gradient has no additional effect on the bending moments that develop.

Step 6: Now, the moment diagrams for the following temperature increments can be easily calculated. For each temperature increment, the new moment resistance for point B is calculated ${}^{T}M_{B,fi,Rd}^{-}$. The moment diagram is constructed setting the moment at the support equal to the resistance moment and redistributing the moments at the spans so that equilibrium is satisfied. If the maximum moment appearing at the span $M_{sp,fi,tot}$, has reached the sagging resistance moment ${}^{T}M_{fi,Rd}^{+}$, then the slab has reached its ultimate load resistance and the fire resistance time has been determined.

The above procedure was applied with a temperature step $\Delta T = 5$ °C. After parametric studies, it was concluded that this value provided a good balance between accuracy and efficiency. With the results of this procedure, the diagram of Figure 7 is constructed which gives the resistance moments $M_{fi,Rd}^{+}$, $M_{fi,Rd}^{-}$ and the design moments $M_{B,fi,tot}$ and $M_{sp,fi,tot}$ for the internal support and for the spans, respectively, as a function of the fire time. The moment at the support reaches the resistance moment at the 15th minute of the ISO fire (Figure 7). After this point, moment redistribution takes place. Since the system becomes statically determinate, the temperature gradient at the cross section of the slab produces thermal

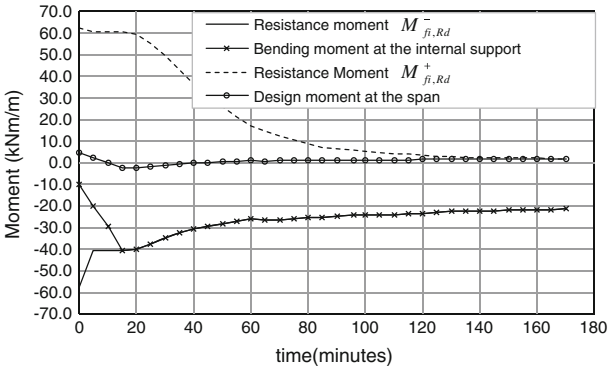

Figure 7. Evolution of the resistances and the design bending moments with time (continuous slab).

bowing only and not additional moments. As the fire continues, the moment increases at the span while both the hogging and sagging resistance moments decrease. At a critical time, both the sagging moment and the hogging moment reach to the corresponding resistance values and the slab becomes kinematically unstable. This happens at the 170th minute of the ISO fire, i.e. the continuous slab has a fire resistance of R170. The procedure and the corresponding moment diagrams are illustrated in Figure 8.

It must be noticed that the fire resistance of the continuous slab is much higher than the fire resistance of the simply supported slab, despite the fact that they have the same load bearing capacities at room temperature. Moreover, this con-

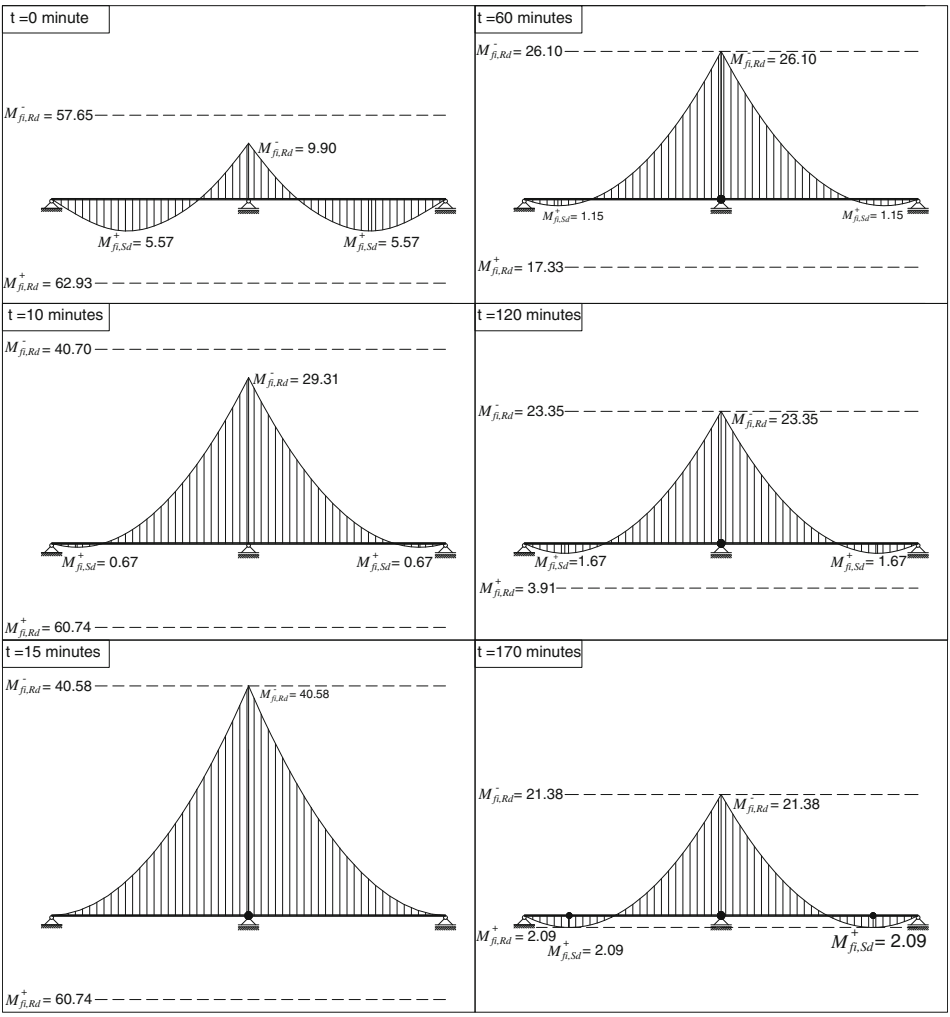

Figure 8. Moment diagrams and resistances for continuous slab in characteristic temperatures (moments given in kNm/m).

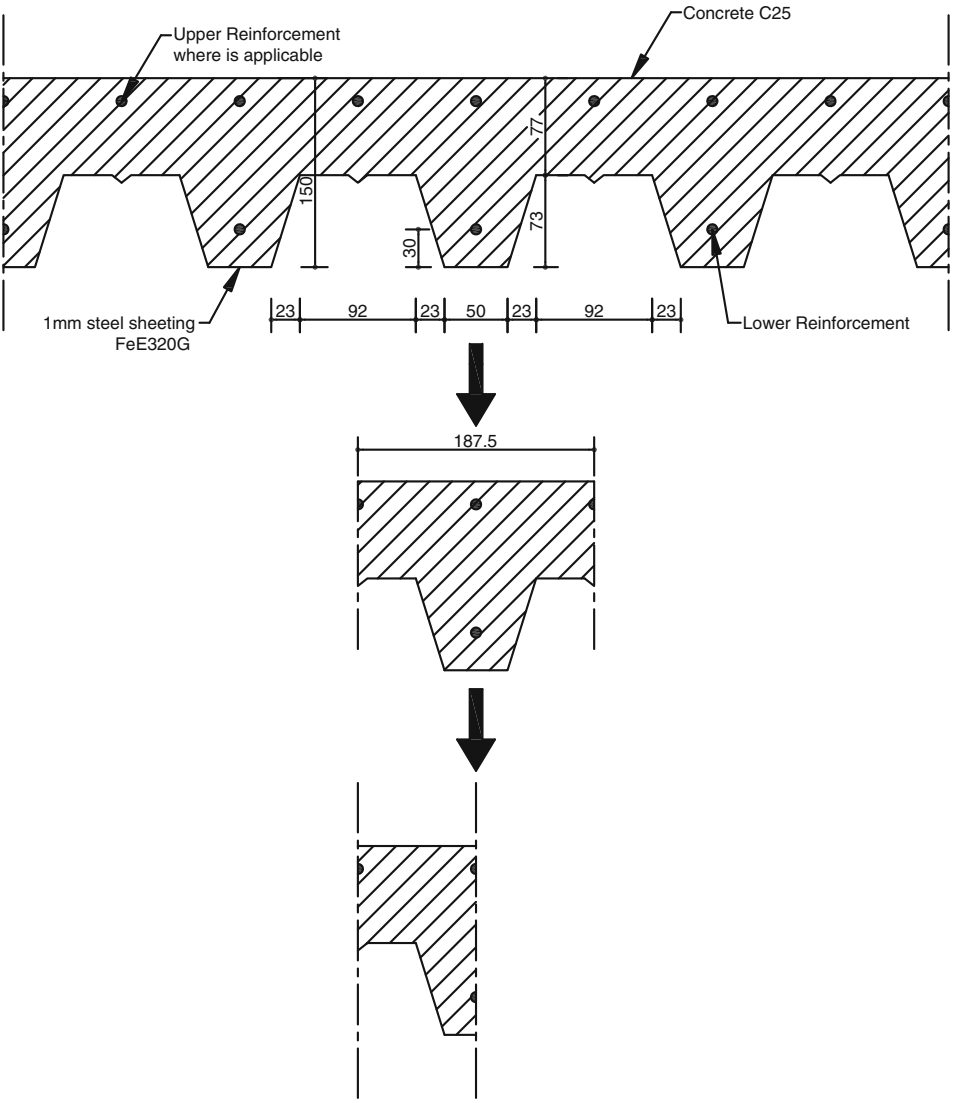

Figure 9. Simplification of the analysis model.

clusion holds despite the unfavorable (at a first glance) effect of the thermal gradient in the case of the continuous slab. Actually, the temperature difference between the upper and the lower side of the composite slab is remarkable even from the first minutes of the fire exposure (at the 15th minute the temperature difference is about 300 °C) and this demonstrates that the thermal gradient effect is important in the case of the continuous slab. The influence of the bending moments due to the thermal gradient is different for the internal support and for the span. At the internal support the design moment reaches quickly the resistance

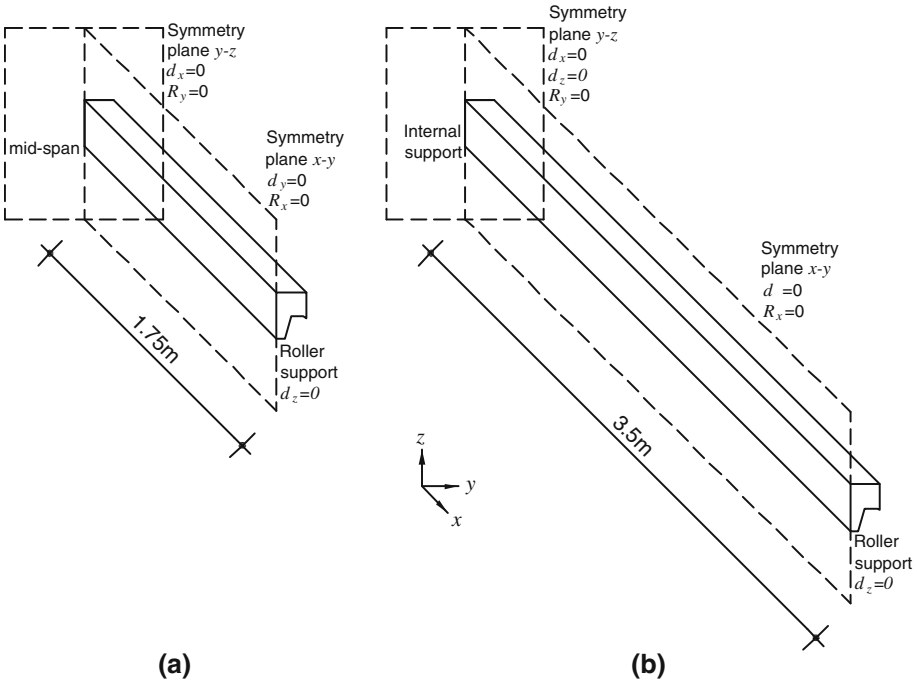

Figure 10. Boundary conditions that are used for the symmetry (not in scale): (a) simply supported beam (b) continuous beam.

moment because the negative moment due to the external loading is enlarged by the negative moment due to the thermal gradient. After the first plastic hinge is formed, moment redistribution takes place and the moment at the support remains equal to the resistance moment, which is, however, modified with time. At the span the moment due to the design load is positive and the addition of the negative moment due to the thermal gradient leads to a reduction of the total value of bending moment. The reduction is considerable and for this reason the collapse is prevented until the 170th minute.

5. The Advanced Calculation Model

5.1. Development of the Numerical Model

The numerical analysis was carried out using the nonlinear finite element code MSC-MARC [20]. Due to the fact that composite slabs are formed using continuous profiled sheeting, it is adequate to simulate a section which is 187.5 mm wide (Figure 9). Moreover, due to the symmetry of this section with respect to the vertical axis, it is adequate to finally model only half of this. For further simplification, as trying to reduce the computational cost which is associated with the nonlinear three-dimensional modeling, only half of the total length of the slab is considered, using the appropriate symmetry boundary conditions. These simplifi-

cations will not affect the results, which will be identical with those of the full model. Therefore, for the simply supported slab, a length equal to 1.75 m is modelled using the following boundary conditions (Figure 10a):

- Fixed displacement $d_y = 0$ and fixed rotation $R_x = 0$ for all the nodes on the x–z symmetry plane.
- Fixed displacement $d_x = 0$ and fixed rotation $R_y = 0$ for all the nodes on the y–z symmetry plane.
- Fixed displacement $d_z = 0$ for the lower edge nodes of the end of the slab corresponding to the roller support.

For the case of the continuous slab the half of the total length is modeled which is equal to 3.5 m. The boundary conditions that are used are the following (Figure 10b):

- Fixed displacement $d_y = 0$ and fixed rotation $R_x = 0$ for all the nodes on the x–z symmetry plane
- Fixed displacements $d_x = 0$ and $d_z = 0$ and fixed rotation $R_y = 0$ for all the nodes on the y–z symmetry plane that coincides with the position of the internal support.
- Fixed displacement $d_z = 0$ for the lower edge nodes of the end of the slab corresponding to the roller support.

The models developed for the simulation of the composite slabs utilize three different types of elements. The steel profile was modeled through four-node shell elements while concrete was simulated with three-dimensional solid elements. The nodes of the shell elements were connected to the corresponding nodes of the 3D-solid elements of concrete (Figure 11). Two-node, 3D frame elements were

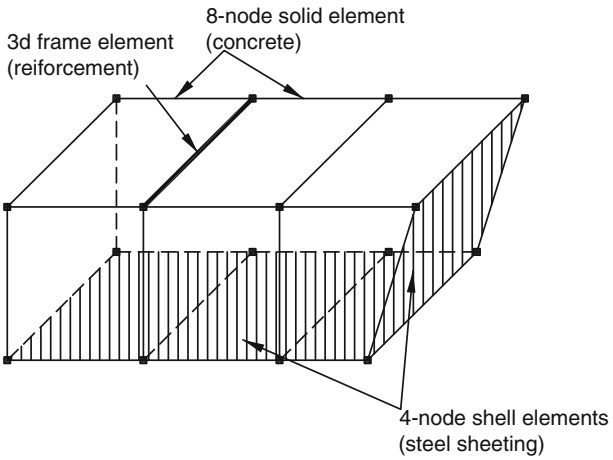

Figure 11. Connection of solid elements with shell and frame elements.

Table 2
The Finite Elements Used for the Representation of the Two Types of Slabs

	Solid elements (concrete)	Shell elements (steel sheeting)	Frame elements (reinforcement)
Simply supported slab	13300	2625	175
Continuous slab	32200	5250	700

used for modeling the reinforcing bars. The numbers of the finite elements used for the representation of the simply supported slab and for the continuous slab are given in Table 2.

The thermal properties of the materials (thermal conductivity and specific heat) are assumed to be temperature dependent as it is defined in [18, 19] for concrete and steel respectively. Moreover, the yield strength of steel, the compressive and tensile strength of concrete and the modulus of elasticity of both materials are temperature dependent.

It should be noted that the advanced numerical model assumes a perfect bond between the steel sheeting and the concrete. Concerning the possible debonding that has been observed during fire tests (e.g. [14, 21]), it is recalled that the phenomenon is local and it has been observed in composite slabs with steel sheeting of considerable height [14]. Moreover, according to the experimental results that are presented in [14, 22], the typical failure mode for fire exposed composite slabs is flexural. The longitudinal shear failure that is observed at room temperature does not usually arise in fire tests. This can be attributed to the fact that the temperature of the steel decking increases rapidly during the fire, its strength is significantly reduced and the tensile forces are undertaken by the reinforcing bars. Therefore, longitudinal shear failure does not seem to be a critical phenomenon during fire exposure and flexural failure is expected. The above remarks fully justify the assumption of the complete bonding between the steel sheeting and the concrete, which has also been adopted by several former numerical studies on the same subject (see e.g. [5, 14, 23]).

5.2. Thermal Boundary Conditions

The following thermal boundary conditions were taken into account (Figure 12).

- Along the symmetry boundaries, adiabatic boundary conditions were considered.
- On the upper side of the composite slab (ambient air side), a solid–fluid boundary condition was considered. In Equation 4 the convective heat transfer coefficient was assumed to be constant and equal to $h_c = 4\ \mathrm{W/m^2\ K}$. Moreover, according to Eurocode 1 [12], the second term of the r.h.s of Equation 4 was ignored.
- On the lower side of the composite slab (fire side), solid–fluid boundary conditions were also considered. According to [12], the convective heat transfer

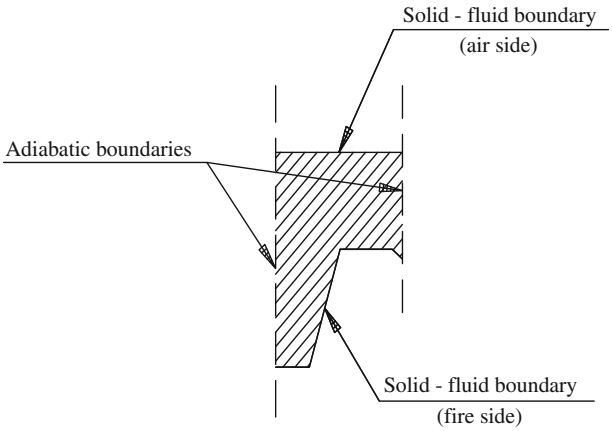

Figure 12. The thermal boundary conditions.

coefficient was assumed to be constant and equal to $h_c = 25$ W/m^2 K. In the second term of the r.h.s of Equation 8 the emissivity of fire ε_f and the emissivity of the construction material ε_m (in this case the corrugated steel sheeting) were considered according to [12]. The parameters were taken as $\varepsilon_f = 1.0$ and $\varepsilon_m = 0.7$ respectively. The view factor of the lower flange of the profiled steel sheeting was taken equal to $\Phi_{l.f.} = 1.0$. The view factors for the web and for the upper flange of the steel sheeting were calculated following the approach first developed in [24] and adopted also by Eurocode 4, Part 1–2 [13]. The calculations for the specific profile used here gave $\Phi_{web} = 0.510$ and $\Phi_{u.f.} = 0.647$ for the web and the upper flange respectively.

Additionally, parametric analyses were conducted in order to investigate if the simplification adopted by Eurocode 1 [12] about the constant value of the convective heat transfer coefficient h_c, affects the heat transfer analysis and, consequently, the mechanical analysis that follows. In the latter, the parameters of Equation 6 were taken according to [15], as $\alpha = 2.2$ and $m = 1/4$ for the upper side of the slab (air side) and $\alpha = 1.0$ and $m = 1/3$ for the lower side of the slab (fire side). In the first analysis series the convective heat transfer coefficient was considered as constant, while in the second analysis series a variable heat transfer coefficient was used.

5.3. Analysis

The numerical analysis for the determination of the fire resistance of the composite slab is a demanding task because various non-linear phenomena evolve during the fire exposure:

- Non-linear material response for both steel and concrete, including the possible cracking of concrete due to its low tensile strength.

- Dependence of all the mechanical and thermal properties of the materials on temperature.
- Convective and radiation heat exchange on the boundaries of the composite slab (lower and upper surfaces). Consequently, a non-linear temperature distribution across the section of the slab arises.

In the present paper, the behavior of the composite slab in elevated temperatures is modeled through combined thermal–mechanical analysis which takes into account all the aforementioned non-linear effects. The temperature increase contributes to the deformation of the slab through thermal strains and also influences the properties of the materials. Actually, a heat transfer analysis is first performed which is followed by a stress analysis.

In this case study the composite slabs are exposed to the standard ISO 834 fire curve for 240 min and the problem is simulated through transient heat transfer under constant imposed load. It is noticed that the loading is applied prior to the increase of the temperature. The temperature distribution is assumed to be constant along the length of the slab. The initial temperature for the composite slab is taken equal to 20 °C.

6. Results of the Numerical Analysis

6.1. Results of the Heat Transfer Analysis

Figure 13 gives the temperatures at characteristic points of the cross-section of the slab. It is noticed that the maximum temperatures that are obtained for the lower flange are close to the corresponding values of the standard fire curve. The temperature at points F and G is quite lower due to the reduced incident thermal radiation on the web and the on upper flange. In the concrete, as the distance from the steel decking is increasing, the temperature decreases. As expected, the

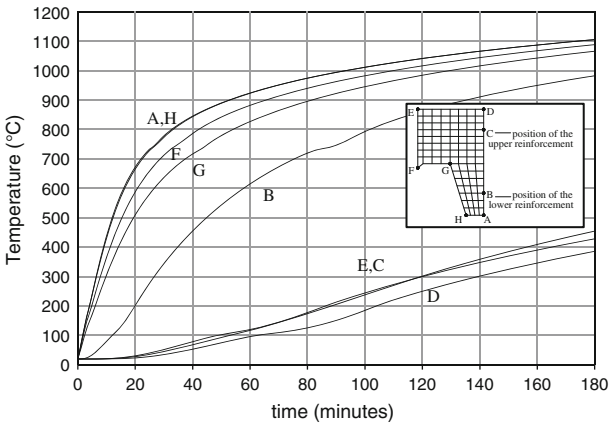

Figure 13. Variation of the temperature in characteristic cross-section points with time.

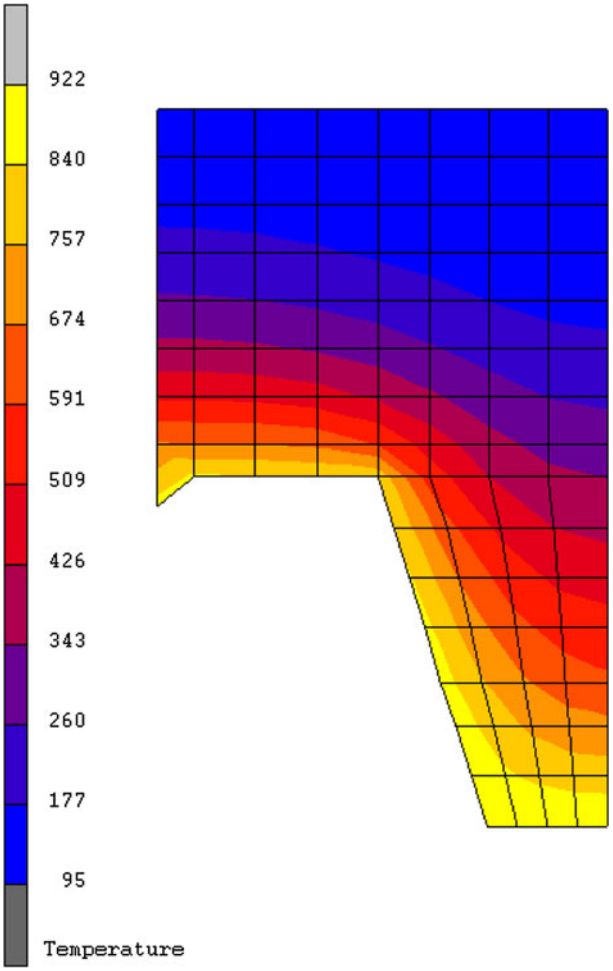

Figure 14. Temperature distribution in the slab cross-section at 60 min.

minimum values are calculated for the upper part of the slab. The temperature of the lower flange of the steel decking after the 20th minute of the analysis (points A, H) is very high.

According to Eurocode 4 [13], the decisive fire resistance time with respect to the maximum temperature rise, is calculated equal to 70 min. For that time the temperature of points E, D at the upper side of the concrete slab does not exceed the value of 180 °C. Therefore, the slab satisfies the ''I'' criterion for thermal insulation.

The temperature distribution that is illustrated in Figure 14 depicts accurately the isotherms of the cross section. The differentiation of the temperature in the horizontal planes is due to the presence of the ribs. The developed temperature

Table 3
Comparison of Numerically Obtained Temperatures in the Composite Slab with Those Obtained Applying the Recommendations of Eurocode 4

	Mean temperature in the numerical model (°C)	Eurocode 4 procedure (°C)	Difference (%)
60 min			
Lower flange	924.368	812.973	13.70
Web	879.262	757.178	16.12
Upper flange	856.877	694.389	23.40
Lower reinforcement	614.768	571.409	7.59
90 min			
Lower flange	994.437	925.316	7.47
Web	964.330	896.351	7.58
Upper flange	943.801	840.145	12.34
Lower reinforcement	746.638	743.480	0.42
120 min			
Lower flange	1041.374	989.946	5.20
Web	1018.830	973.045	4.71
Upper flange	1001.067	924.332	8.30
Lower reinforcement	861.595	844.705	2.00

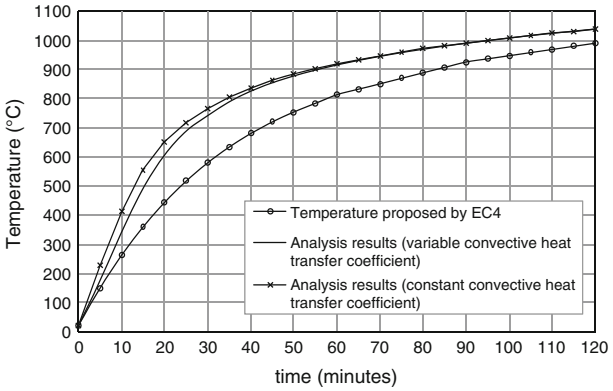

Figure 15. Development of mean temperature of the lower flange of the steel sheeting with time.

pattern is absolutely similar with the one that is indicated in [13, Figure D.3.2.a], however, the temperature values present some differences. Table 3 gives the comparison between the numerically obtained results for the temperatures of the various parts of the profiled steel sheeting and of the lower steel reinforcement, with respect to those obtained by applying the procedures of Eurocode 4 [13] for the same problem. It is noticed that the values of temperature resulting from the heat transfer analysis are greater with respect to those obtained by applying Eurocode 4. For the steel reinforcement the differences are quite small. However, significant

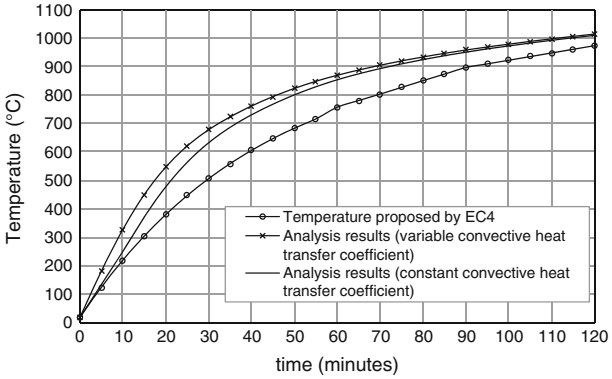

Figure 16. Development of mean temperature of the web of the steel sheeting with time.

differences are observed for the temperatures of the steel sheeting. In this respect, it seems that the procedures of Eurocode 4 are not on the safe side for the type of corrugated steel sheeting used in this paper.

Figures 15 and 16, give the comparison between the results obtained by the two series of heat transfer analyses (the series adopting the variable convective heat transfer coefficient and the series adopting the constant one). More specifically, the mean temperatures obtained for the lower flange (Figure 15) and for the web (Figure 16) are compared. In the same figures, the corresponding values obtained by the application of Eurocode 4 [13] are presented. It is clear that for both cases the results of the numerical analyses are very close. It has to be noticed that after the 60th minute the results coincide. Thus, it is obvious that the simplification adopted by Eurocode 4 [13] for the constant value of the convective heat transfer coefficient is reasonable, as the usage of the more accurate description of h_c leads to almost the same results. Moreover, this fact indicates that the solution of the coupled thermo-mechanical problem is not affected by this parameter.

6.2. Results of the Mechanical Analysis

The curves of Figure 17 give the evolution of the maximum vertical displacement of the two types of slabs with respect to time. For the case of the simply supported composite slab, the collapse occurs at the 67th minute. The response of the continuous composite slab is completely different and it finally collapses at the 226th minute. In both cases, just before collapse occurs, significant deformations at the span are observed. The difference in the response was explained in detail in the previous section and lies mainly on the moment redistribution that takes place during the fire exposure in the case of the continuous slab. Also, in this case, the temperature gradient at the cross-section of the slab affects in a positive way the mechanical problem. In both cases, the contribution of the profiled steel sheeting in the resistance of the composite slab is quite limited in elevated temperatures. Moreover, it is noticed that in both cases the values of the maximum vertical

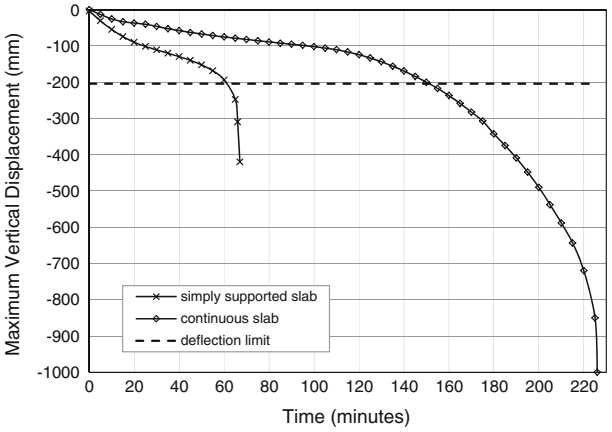

Figure 17. Development of the maximum vertical displacement with time.

deflections of the composite slabs are significantly increased in elevated temperatures. In practice, deflection limits are imposed in order to avoid excessive deformations [25]. For the flexural members the limit value that is usually used is

$$\delta_{\max} = \frac{L^2}{400d}, \tag{8}$$

where d is the depth of the section and L is the length of the span. The application of the above criterion for the cases treated here gives $\delta_{\max} = 204$ mm. This occurs around the 62nd minute for the simply supported slab, while the continuous slab reaches the limit deflection approximately at the 152nd minute. Another limitation for the flexural structural members that is referred to DIN 4102 [26] is the rate of deflection. This criterion is expressed in the form

$$\frac{du}{dt} \leq \frac{L^2}{9000d}, \tag{9}$$

where du is the change in deflection (mm) during a time interval dt of one minute. Figure 18 presents the calculated deflection rate for the two slab systems. In the cases treated here, the limiting rate of deflection is calculated to be 9.07 mm/min. For the simply supported slab, this limiting rate is reached in the 62nd minute, while in the case of the continuous slab this happens approximately at the 20th minute.

Figure 19 illustrates the deformed shape of the simply supported slab and the equivalent cracking strain at the 30th and 67th minutes of analysis. The development of cracking starts rather early. At the time of 30 min various cracks have already been formed in the composite slab. As the time increases, the cracking

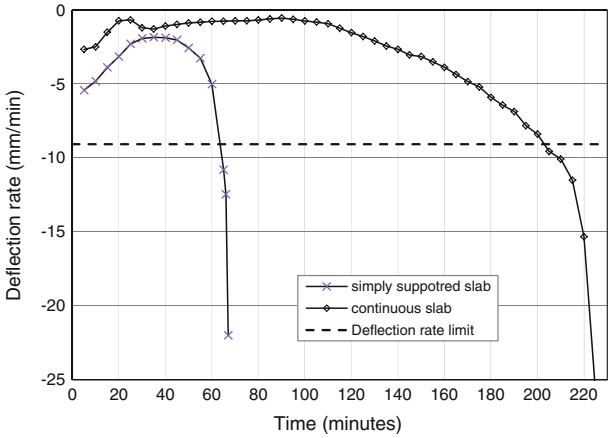

Figure 18. Development of the deflection rate with time.

develops towards the upper side of the slab. Significant cracking is noticed also in the interface between the concrete and the steel reinforcement.

For the case of the continuous slab, the deformed shape and the cracking strains are illustrated in Figure 20. The left part of the figure corresponds to the internal support of the slab. At the time of 60 min various distinct cracks have already developed at the upper part of the slab near the support. However, even at the time of the 120 min, the cracking at the lower part of the slab is very limited along the span, indicating that the values of the sagging moments are still very low. The situation is different at the 180 min and the significant deformations are obvious. Significant cracking appears in the vicinity of the support and at the mid-span. This is a sign that the resistances of the slab are progressively exhausted. The above findings compare well with the corresponding results of the simplified model, as they are expressed through the diagrams of Figure 8.

Finally, it is interesting to compare the results, in terms of obtained fire resistance between the simplified and the advanced models. It has to be noticed first that a direct comparison between them is not possible, because the fire resistance in the simplified models is defined through the attainment of the ultimate strength of the structural systems while in the case of the advanced models the fire resistance is defined through maximum deflections or deflection rates. However, some qualitative comparison is still possible.

In Sect. 4.1, the simply supported slab was found to have, according to Eurocode 4 [13], a load bearing capacity for 77 min. On the other hand, the collapse of the corresponding numerical model (as it is indicated in Figure 17) occurred in the 67th minute. It can be easily verified by studying all the displayed results that the main reason for this difference is the fact that the temperature values calculated for the steel sheeting following Eurocode 4 [13] are lower compared with the respective values that result from the thermal analysis. Therefore, the sagging moment resistance is greater in the case of the simplified model.

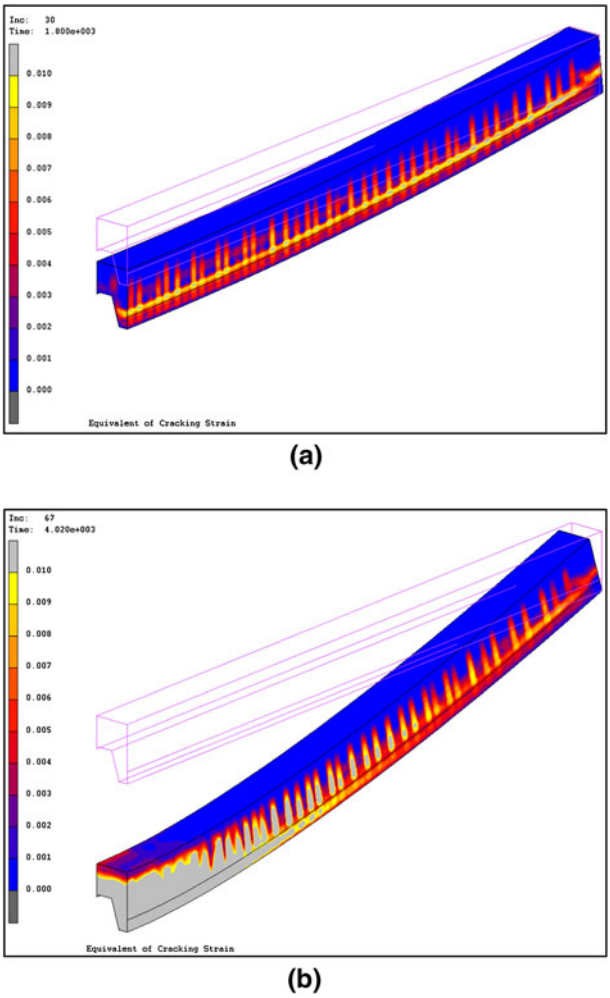

Figure 19. The deformed shape of the continuous composite slab and the corresponding cracking strains; (a) at the 30th minute, (b) at the 67th minute.

The resistance of the continuous slab seems to be dominated by the effects of the temperature gradient and by the stress redistribution that takes place when the resistance at the position of the internal support is exhausted. In Sect. 4.2, the continuous slab was found to have, according to Eurocode 4 [13], fire resistance for 170 min. On the other hand, the numerical analysis indicated that the failure occurs at the 226th minute. At a first glance this difference seems striking, however, it should be examined having in mind all the simplified assumptions included in the simplified model. More specifically, in the simplified model the ultimate

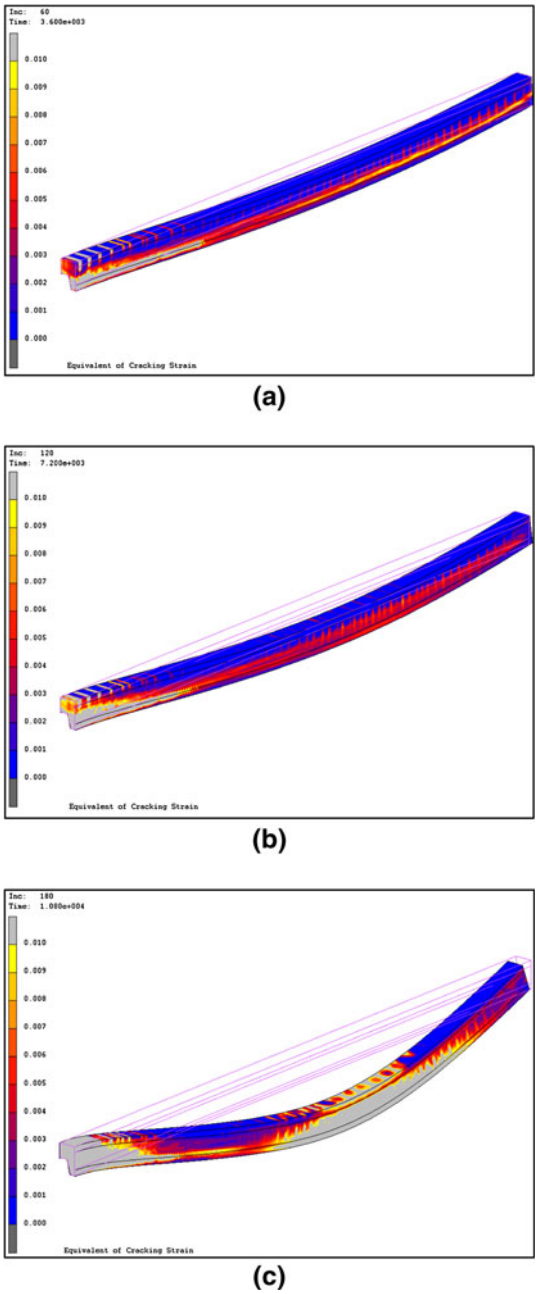

Figure 20. The deformed shape of the continuous composite slab and the corresponding cracking strains; (a) at 60th minute, (b) at 120th minute, (c) at 180th minute.

Table 4
Comparison of the Fire Resistance Times

	Simply supported slab	Continuous slab
Simplified model	77 min	170 min
Advanced calculation model—strength	67 min	226 min
Advanced calculation model—deflection limit criterion	62 min	152 min
Advanced calculation model—rate of deflection criterion	62 min	203 min

state was achieved when the moment resistance at mid-span became equal to the design moment (at the 170th minute) leading to an unstable system, while in the numerical model the failure was indicated by the inability of the solution procedure to converge to a solution due to large strain increments. Of course, the above two failure criteria are not directly comparable. One more reason making comparisons very delicate in this situation, is the fact that the ISO curve temperature at the 170th minute is 1,101 °C, while at the 226th minute it is 1144 °C, i.e. the temperature differences become very small as the time increases, making the accurate estimation of the failure state in terms of strength a very delicate issue. Except the above, it should be reminded here that the calculation of moment resistances in the case of the simplified models was based upon certain simplifications introduced by Eurocode 4 with respect to the calculation of the temperatures of the components of the composite slab. Following the code, the temperatures were assumed to be uniform along the horizontal zones of the concrete. Moreover, each part of the steel sheeting (upper flange, web and lower flange) is supposed to have a uniform temperature. The above are illustrated in Figure 3. Obviously, as it results from the plot of Figure 14, this assumption is not absolutely correct and may lead to some differences in the bending moment resistances that are calculated by the two methods. Table 4 summarizes the obtained fire resistances for both structural systems, in the time domain.

7. Conclusions

The paper presents the accurate thermo-mechanical modeling of the behavior of a simply supported and of a continuous two-span slab, which are submitted in elevated temperatures according to the standard ISO fire curve. The numerical models are based on combination of three dimensional finite elements for the concrete, shell elements for the profiled steel sheeting and frame elements for the steel reinforcement. All the necessary mechanical and thermal boundary conditions are taken into account and symmetry procedures are applied in order to reduce the dimensions of the numerical problem. In parallel, the same problems are studied through simplified methods based upon the recommendations of Eurocode 4 for the determination of the temperatures of the various parts of the composite slab

and for the calculation of the sagging and hogging moment resistances. An algorithm is introduced, that facilitates the determination of the fire resistance time within this simplified framework.

The main conclusions of the study are the following:

- The continuous slab seems to have a significantly improved behavior in elevated temperatures with respect to the simply supported one. This result is verified by both the simple and the advance solution procedures.
- The temperatures obtained by means of the advanced thermal analysis are higher compared to the ones determined by means of the simplified procedures specified in the Eurocodes. The differences are more significant for the thin-walled steel sheeting and may lead to fire resistance times which are smaller compared to the ones calculated through Eurocode 4. For the case of the simply supported slab, if deflection limits are respected, this reduction is of the order of 5 min. For the case of the continuous slab, the definition of fire resistance time for the advanced model depends strongly on the applied criterion. The strictest criterion in the case examined here was found to be the one related with the deflection. The fire resistance time determined according to this criterion is in rather good agreement with the one calculated through the simplified model which is based on strength (152 min and 170 min respectively).

Acknowledgments

This research has been co-financed by the European Union (European Social Fund–ESF) and Greek national funds through the Operational Program ''Education and Lifelong Learning'' of the National Strategic Reference Framework (NSRF)—Research Funding Program: Heracleitus II. Investing in knowledge society through the European Social Fund.

Appendix: Validation of the Numerical Model

The validation of the numerical model proposed in this study is based on the experimental results that are reported by Hamerlinck in [14]. During this experimental program, fire tests were conducted in order to investigate the behavior of composite slabs during exposure to standard fire. The verification of the current advanced model is based on test No.2, as it is referred in [14], which is a fire test on a simply supported, one-way composite slab (similar to the one studied in this paper).

The total span of the test specimen is equal to 3.2 m, as it is illustrated in Figure 21. The test is performed on a slab with Prins 73 steel sheeting with thickness equal to 1 mm. The self-weight of the slabs is $G = 2.7$ kN/m^2, while the imposed load is equal to $Q = 3$ kN/m^2. The loading was applied by four point loads (see Figure 21). The positive reinforcement is equal to Ø10/208 while the negative one is Ø6/150 and they are defined as hot-rolled and cold worked respec-

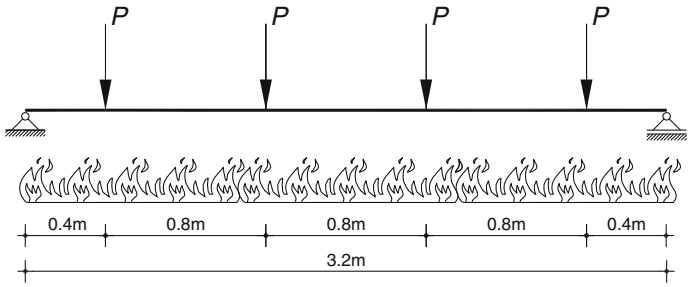

Figure 21. The test specimen and the arrangement of the loading (test No. 2 of [14]).

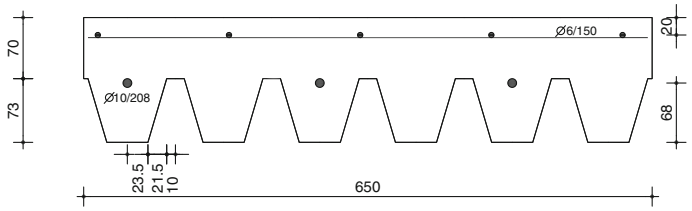

Figure 22. The cross section of the slab (all the dimensions in mm).

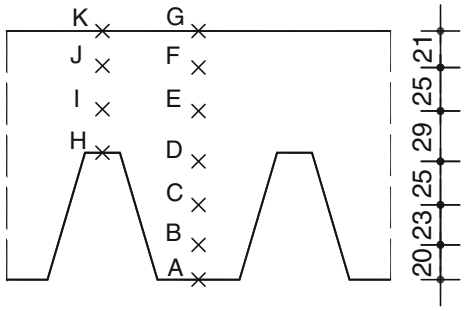

Figure 23. The positions of the thermocouples.

tively. The concrete depth which is equal to 173 mm. During the fire test, thermocouples were used for the measurement of the temperature of the steel sheeting, of the reinforcement and of various points in concrete. The accurate dimensions of the cross-section and the arrangement of the reinforcing bars are illustrated in Figure 22 while the position of the thermocouples is presented in Figure 23. The mechanical properties of steel and concrete were measured at room temperature during the experimental program and they are presented in Table 5.

Table 5
Measured Mechanical Properties of Steel and Concrete at Room Temperature (Test No. 2 of [14])

Steel	Yield stress	Ultimate stress
Ø6 (hot-rolled)	552 MPa	598 MPa
Ø10 (cold-worked)	587 MPa	677 MPa
Steel sheeting	306 MPa	384 MPa
Concrete	Compressive stress	Tensile stress
C25	33.6 MPa	3.5 MPa

The finite element model that is developed in order to compare the numerical with the experimental results follows all the principles that were described in Sect. 5.2. All the mechanical and thermal material properties are assumed to be temperature dependent according to [18, 19] for concrete and steel respectively. The material characteristics measured during the experimental program are taken into account. Moreover, the appropriate distinction is made for hot-rolled and cold-worked steel.

The thermal boundary conditions are considered in the same way as they were presented in Sect. 5.2. For the emissivities, the values used in [14] were adopted. Finally, it is noted that the analysis takes into account all the considerations that were described in Sect. 5.3.

The comparison of the numerical and the experimental results, considering the thermal response, is illustrated in Figure 24. In general, a good agreement between the measured and calculated values is observed.

Considering the evaluation of the mechanical response of the slab, it is noted a very good agreement between the measured and the calculated deflections until the 97th minute of the fire exposure (Figure 25). After this minute the numerical analysis stops due to numerical problems attributed to the significant cracking of concrete.

In general, it can be concluded that the numerical model represents accurately both the thermal and the mechanical response of the studied composite slab under fire conditions.

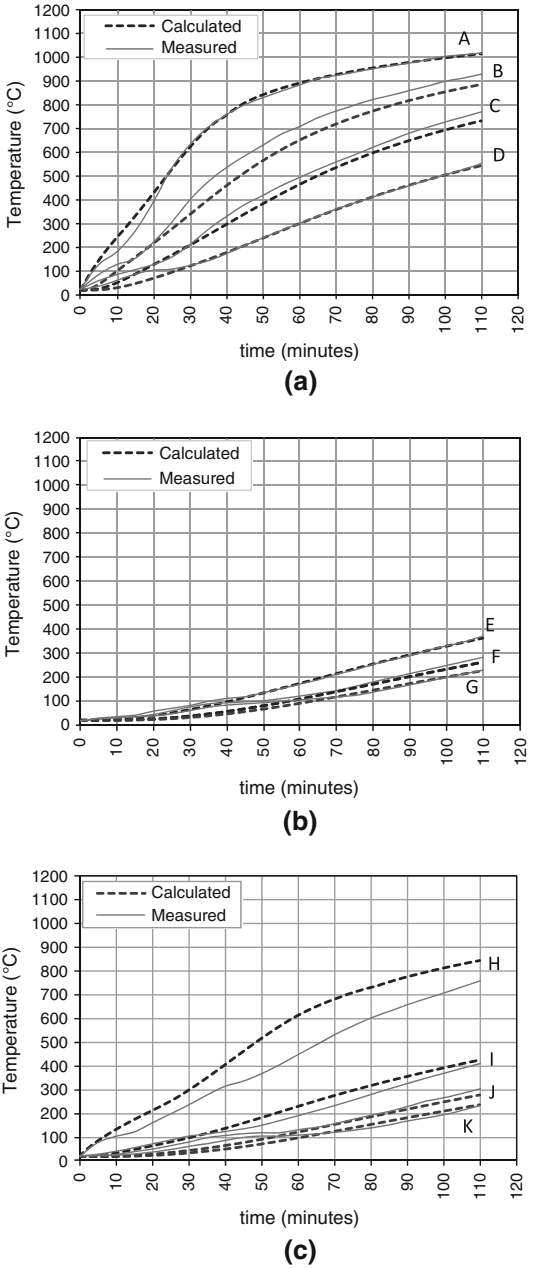

Figure 24. Measured and calculated temperatures in the slab.

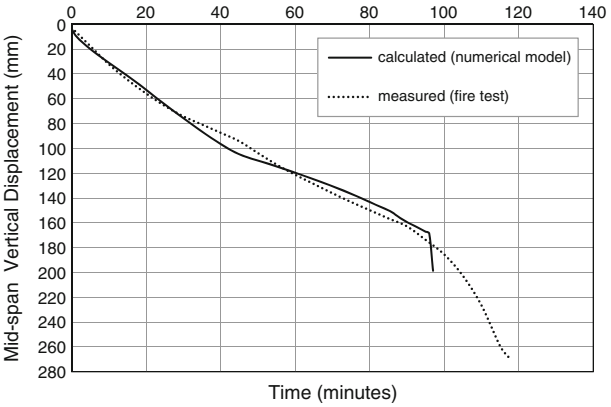

Figure 25. Development of mid-span deflection with time. Comparison between numerical and test results.

References

1. Thomson GC, Moxon K, Preston RR (1987) Contract report to steel construction institute. Indicative fire test on composite concrete/steel deck floor system
2. The Steel Construction Institute (2008) Report to corus CSD. slimflor compendium. Document RT1147 Version 01
3. Bailey CG, White DS, Moore DB (2000) The tensile membrane action of unrestrained composite slabs simulated under fire conditions. Eng Struct 22:1583–1595
4. Hamerlinck AF, Twilt L, Brekelmans JWPM, Van de Haar PW (1990) The mechanical behaviour of fire-exposed composite steel/concrete slabs under negative bending. Test report, Research report BI-90-118, Eindhoven University of Technology/TNO-Building and Construction Research
5. Gille M, Usmani A, Rotter M, O' Connor M (2001) Modeling of heated composite floor slabs with reference to the Cardington experiments. Fire Saf J 36:745–767
6. Huang Z, Burgess I, Plank R (2000) Effective stiffness modeling of composite concrete slabs in fire. Eng Struct 22:1133–1144
7. Vulcan (2008) Vulcan Solutions Ltd, http://www.vulcan-solutions.com/index.html
8. Yu X, Huang Z, Burgess I, Plank R (2008) Nonlinear analysis of orthotropic slabs in fire. Eng Struct 30:67–80
9. Gillie M, Usmani AS, Rotter JM (2001) A structural analysis of the first Cardington test. J Constr Steel Res 57:581–601
10. Lamont S, Usmani AS, Drysdale DD (2001) Heat transfer analysis of the composite slab in the Cardington frame fire tests. Fire Saf J 36:815–839
11. Cashell KA, Elghazouli AY, Izzuddin BA (2011) Failure assessment of lightly reinforced floor slabs. II: analytical studies. J Struct Eng-ASCE 137:989–1001
12. European Committee for Standardization (2002) Eurocode 1. EN 1991-1-2.General actions-actions on structures exposed to fire—Part 1–2. General actions-actions on structures exposed to fire
13. European Committee for Standardization (2003) Eurocode4. EN 1994-1-2. Design of composite steel and concrete structures. Part 1–2. General rules—structural fire design

14. Hamerlinck AF (1991) The behaviour of fire exposed composite steel/concrete slabs. PhD thesis, Eindhoven University of Technology
15. Wang YC (2002) Steel and composite structures: behavior and design for fire safety, 1st edn. Spon Press, London
16. European Committee for Standardization (2002) Eurocode 0. EN 1990. Basis of structural design
17. Franssen JM, Vila Real P (2010) Fire design of steel structures, 1st edn. Ernst & Sohn, Berlin
18. European Committee for Standardization (2002) Eurocode 2. EN 1992-1-2. Design of concrete structures—Part 1–2. General rules—structural fire design
19. European Committee for Standardization (2003) Eurocode 3. EN 1993-1-2. Design of steel structures—Part 1–2. General rules—structural fire design
20. MSC Software Corporation (2010) MSC Marc, vol A: theory and user information, Version
21. Newman GM, Robinson JT, Bailey CG (2000) Fire safe design: a new approach to multi-story steel-framed buildings. The Steel Construction Institute, Berkshire (UK)
22. Both C (1998) The fire resistance of composite steel-concrete slabs. PhD thesis, Eindhoven University of Technology
23. Lim L, Buchanan A, Moss P, Franssen JM (2004) Numerical modeling of two way concrete slabs in fire. Eng Struct 26:1081–1091
24. Wickström U, Sterner E (1990) TASEF, temperature analysis of structures exposed to fire-user's manual. Swedish National Testing Institute, SP report 05
25. Purkiss JA (2007) Fire safety engineering—design of structures, 2nd edn. Butterworth—Heinemann, Oxford
26. DIN 4102—Part 2 (1977) Fire behavior of building materials and building components. Building components definitions, requirements and test